

Effect of Using Nanoscale Titanium as a Target Instead of a Bulk Target on Laser-Induced Plasma Properties

Muntazar shihab Ahmed

Laser science and technology, Department of Applied Sciences, University of Technology, Baghdad, Iraq.

Haider Abdulrida

Laser science and technology, Department of Applied Sciences, University of Technology, Baghdad, Iraq.

Qusay Adnan Abbas

Laser science and technology, Department of Applied Sciences, University of Technology, Baghdad, Iraq.

Email: as.20.72@grad.uotechnology.edu.iq, 100329@uotechnology.edu.iq, Qusay.a@Sc.Uobaghdad.edu.iq

Abstract

In this work, the effect of the target configuration as nano or bulk-titanium target on the plasma emission and plasma parameter induced by Q-switched nanosecond Nd: YAG laser at different energies under vacuum was studied. The effect of laser energy (200, 300, and 400 mJ) on the parameter of the induced plasma was studied. The plasma number density was enhanced for the nano target compared with the bulk one, while the plasma temperature slightly increased. The Keldysh parameter indicates that the ionization from the titanium targets occurs through the multiphoton process. Using the nano target enhanced the LIPS intensity due to the different laser-matter interaction mechanisms of the nano-target compared with the bulk target. This technique can be used effectively for enhancing the breakdown spectroscopy, especially for targets of low absorption

Keywords: Plasma emission, LIPS, Nano target, plasma characteristics.

Introduction

Plasma is a quasi-neutral media that contains charged and neutral particles and exhibits collective behavior [1]. Plasma can be categorized allowing to its characteristics such as its number density and average kinetic energy as cold or hot plasma [2]. As a result of plasma complexity, due to its large number of interactions between different species, there are different types of modeling, such as particle and fluid models, that describe the plasma to explain the behavior in the glow discharge [3].

Optical Emission Spectroscopy (OES) is a popular analytical technique that has wide-ranging applications. It is a frequently used analytical method for figuring out the elemental makeup of a variety of materials. Recent research has shown that this technique is widely employed in analyzing samples such as steel, alloy, metal, geological, biological, and environmental. Laser-induced plasma is one of the most popular methods to create plasma from solid surfaces for the OES purpose. Additionally, the vacuum must be used during

plasma etching to avoid the deposit of undesired impurities. The OES technique is used in a most versatile physical method for producing metal nanoparticles by pulsed laser ablation [4]. In which, the characteristics of the prepared nanoparticles can be controlled by varying the plasma parameters [5]. In plasma-nanoparticles interaction, due to the decreased thermal conductivity of tiny particles exposed to laser irradiation, so, surface nanoparticles and surface roughness might increase the ablation efficiency by lowering the ablation threshold [6]. As a result, NPs are perfect thermally insulated defects capable of lowering the breakdown threshold, especially at low laser irradiation. High-energy laser pulses, on the other hand, can create electric fields that are potent enough to cause direct emission of electrons from the surface. Due to a significant local increase in the electromagnetic field of the incident light, this phenomenon, which is well-known in electrical discharges in a vacuum, can occur under laser irradiation when the metallic surface is composed of nanostructures [7]. However, all plasma processes of laser-induced plasma are highly dependent on the surrounding media, and pressure during the irradiation, in addition to laser parameters such as laser fluence, wavelength, and pulse duration [8].

Sherbini et al. 2019 [9] discussed the signal enhancement of laser-induced plasma by nanoparticles. They use Nd: YAG laser to produce breakdown at the target surface of different types of nanomaterial (Zn, Ag, Si, Ti, Al, and Fe) to investigate the effect of NPs size, laser wavelength, and fluence, to obtain stronger signals than their corresponding bulk samples. Modeling of the measurements interprets the occurrence of enhanced detectability of atomic species in biological and chemical synthesis. Fikry et al, 2020 [10] investigated the impact of a suitable pairing of

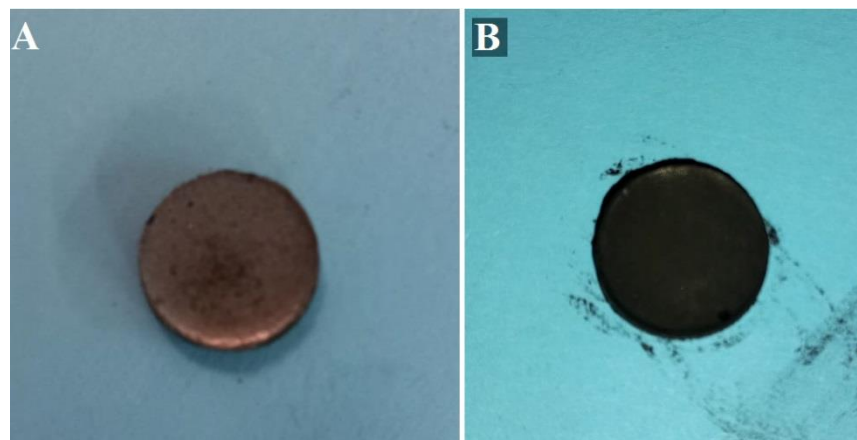
laser wavelengths and pulse energy on the generated plasma characterization using 266, 355, 532, and 1064 nm laser wavelengths. LIPS created a plasma plume from a copper target with a single shot of 170 ps at various laser fluences. Hameed et al, 2022 [11] studied the emission lines of LIPS from three metallic targets (Cu, Ti, and Ni) with laser pulses in air. The electron temperature was determined using the ratios method. Electron temperature was in the ranges 0.34-0.44 eV, 0.28-0.42 eV, and 0.34-0.45 eV for Cu, Ti, and Ni respectively at 70 MW laser power.

In this work, we study the plasma characterization induced by Q-switched nanolaser from titanium targets of different features (Nano, and bulk Ti samples) at different laser energy. The investigation includes determining the difference in plasma parameters under vacuum.

2. Experimental

Two types of titanium were used in this work to study the plasma emission induced by plasma, nano-titanium powder with average particle diameter of 50 nm of 99.9% purity from Sigma-Aldrich Co. and Titanium Plate of 0.5 mm thickness of 99.995% purity Sigma-Aldrich Co.

The powder target was prepared by pressing 2 g of nano-Ti particles as a pellet of 1 cm diameter into a stainless steel mold, using a hydraulic piston under 5 tons press for 10 minutes to be as dense and homogenous as possible. The titanium plate was cut into size of 1×1 cm² and edges were smoothed, and their surfaces were polished by three steps of polishing and then were cleaned with acetone by ultrasonic cleaner followed by pure alcohol about fifteen minutes. Figure 1 shows the two different targets that prepared for used in laser induced plasma spectroscopy (LIPS).

Figure 1: The two different targets (A) bulk and (B) nano titanium targets.

The laser-induced plasma spectroscopy (LIPS) apparatus consists of a nanosecond Q-switched Nd:YAG laser source, and a spectrometer connected to a computer for data collection. Nd:YAG laser work at fundamental wavelength (1064 nm), 10 ns pulse duration, and 2 mm spot diameter was used as source for the LIPS experiment. The laser beam is focused onto the target's surface utilizing a quartz lens at its focal length of 10 cm. The device consists of an external handy piece, power supply, controller, and cooling system using distilled water. The used pulsed laser energies in this work are 200, 300, and 400 mJ.

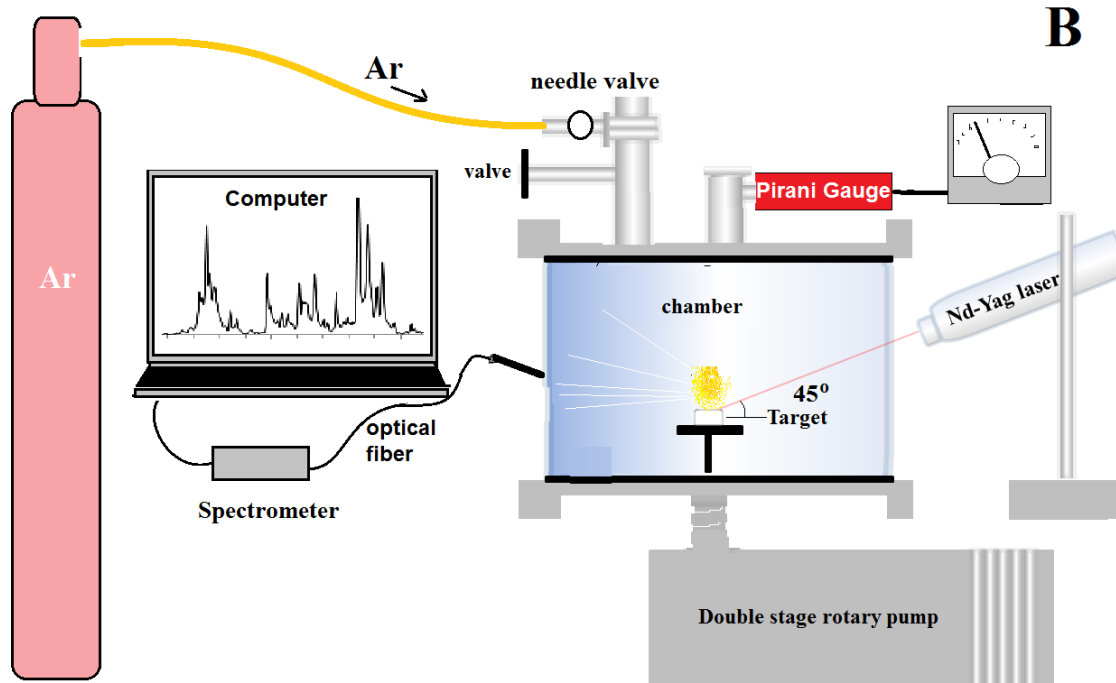
Optical emission spectroscopy diode-array type was used in plasma diagnostics. It is a fast technique of low power requirements for efficient diagnosis of plasma behavior and their parameters. In general, The light ray is collected into fiber optic, which was set at an angle of about 45° degrees to the laser beam axis, and transmit to the instrument (1). The light is analyzed into its components by a diffraction grating (2). The light falls on an array of photodiodes (3), each of which responds only to the narrow range. The diodes are connected to a charge-coupled device (CCD) (4) that convert the light into electrical signal by photovoltaic phenomena. The digital counts are sent to a dedicated computer with spectrum analysis software. The acquired spectrum is immediately displayed on the

screen and saved in computer files. In our work an optical emission spectrometer. Thorlabs compact spectrometer, (Type CCS 100/M) was used in this work. The spectrometer has a high resolution depending on grating used within the wavelength range (320 – 740 nm) with resolution $\Delta\lambda < 0.5 \text{ nm}$, Slit: 20 μm . Figure 3.4 displays Thorlabs spectrometer and the Diode-array spectrometer component.

The pulsed laser was used to create plasma discharge from the prepared targets. The spectrum of the plasma emissions were used to study the effect of changing the target type, laser energy, and surrounding environment. The experiment was repeated for different time under vacuum, and in Ar at 8×10^{-2} Torr pressure. The vacuum was done by a rotary pump model CIT-ALCATEL Annecy, while a Perini gauge type Edward (made in England) was used to measure the vacuum pressure of the chamber. The two types of titanium targets (nano, and Bulk) were put on the target holder. The laser beam was focused onto the target and the emission spectra were acquired utilizing the optical fiber and the spectrometer. The optical fiber of the spectrometer was fixed at constant distance (5cm) from the target. To characterize the plasma properties, the findings of spectral lines for particular species and matched with the data from National Institute Standard Technology NIST database [12]. The

experiment were repeated inside a vacuumed glass chamber as shown in Figure 2.

Figure 2 : Schematic of the experimental arrangement.



The structural Properties of the prepared targets were examined using the X-ray diffraction technique (Shimadzu XRD 6000). A monochromatic wavelength of x-ray ($\lambda=1.5405 \text{ \AA}$) is generated in the x-ray tube from Cu ($K\alpha$) transition using 30 mA current and 40 kV voltage. The scanning was performed at 2θ value in the range (20° - 80°) and speed of 5.00 (degree /min).

3. Results and discussions

Figure 3 shows the X-ray diffraction pattern for the titanium bulk and nano-Ti targets. Polycrystalline structure with many peaks located at about $2\theta=35^\circ, 38^\circ, 40^\circ, 53^\circ, 63^\circ, 70^\circ, 74^\circ, 76^\circ,$ and 77° corresponding to crystalline planes (100), (002), (101), (102), (110), (103), (200), (112), and (201) for the two samples corresponding to the standard card of hexagonal crystalline titanium (JCPDF No. 96-900-8518) without any additional phase,

indicating the targets purity. The XRD pattern for the titanium pellet prepared from nano-powder of diffraction lines appeared broader than the bulk (indicate its nano crystallinity) and with small variation in peaks locations indicate on the existence of some lattice strain. As shown in Table 1, the inter-planer distances (d_{hkl}) were determined according to Bragg formula [13]

$$n \lambda = 2 d_{hkl} \sin \theta \quad \dots \dots \dots (1)$$

where (θ) is the diffraction angle, λ is the x-ray wavelength, and n is the diffraction order.

The full width at half maxima (FWHM) of the diffraction lines were determined by Lorentzian fit. The crystallite sizes was determined according to the Debye-Scherer formula [14]:

$$C.S = \frac{0.9\lambda}{\beta \cdot \cos(\theta)}$$

where β is the line breadth at half maxima (in radian).

..... (2)

Figure 3: The XRD pattern for the nano and bulk -Ti target compared with the standard lines.

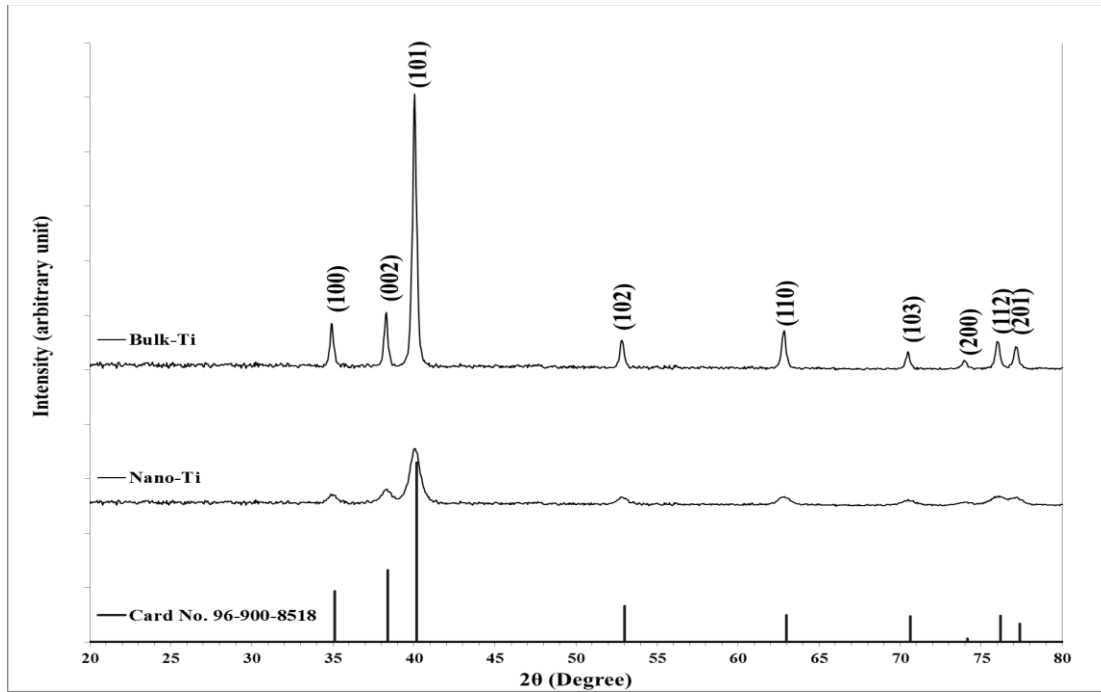


Table 1: XRD parameters for the nano and bulk -Ti targets.

Sample	2 θ (Deg.)	FWHM (Deg.)	d_{hkl} Exp.(Å)	D (nm)	hkl
Bulk	34.9310	0.2500	2.5665	33.3	(100)
	38.2843	0.2630	2.3491	32.0	(002)
	40.0423	0.2900	2.2499	29.2	(101)
	52.8366	0.2950	1.7313	30.1	(102)
	62.8312	0.2870	1.4778	32.4	(110)
	70.4818	0.3020	1.3350	32.2	(103)
	73.9652	0.3050	1.2805	32.6	(200)
	76.0162	0.3240	1.2509	31.1	(112)
	77.1557	0.3360	1.2353	30.2	(201)
Nano	34.9562	0.6400	2.5647	13.0	(100)

38.3095	0.7340	2.3476	11.5	(002)
40.0675	0.7300	2.2486	11.6	(101)
52.8618	0.7640	1.7306	11.6	(102)
62.8564	0.8040	1.4773	11.6	(110)
70.5070	0.9730	1.3346	10.0	(103)
73.9904	0.8890	1.2801	11.2	(200)
76.0414	1.0580	1.2506	9.5	(112)
77.1809	0.8460	1.2350	12.0	(201)

The (100) and (002) planes were selected to calculate the lattice constants for hexagonal structure of Ti crystals according to the relation [15]

$$\frac{1}{d_{hkl}^2} = \frac{4}{3} \frac{h^2 + hk + k^2}{a^2} + \frac{l^2}{c^2}$$

..... (3)

And the lattice strain using [16]:

$$\varepsilon = \frac{\beta \cos\theta}{4}$$

..... (4)

Table 2 illustrates the variation of lattice constants (a and c) for the hexagonal Ti, average crystallite size, and average lattice strain, calculated from equation 2.13, for the three targets of titanium. The lattice constants (a and c) are very close to their values in the standard card. The both of lattice constants slightly decreased for micro-sample compare with the Ti- Bulk and more decreased for nano-sample as a result of increasing the lattice strain due to reducing the crystalline size.

Table 2: Variation of XRD parameters for the different targets.

Sample	a (Å)	c (Å)	Average D(nm)	Average strain
Bulk Ti	2.9636	4.6982	31.4585	0.0011
Nano Ti	2.9615	4.6952	11.3310	0.0031

Figures 4 and 5 show the spectroscopic emission patterns induced by laser in air under 8×10^{-2} Torr vacuum at different laser energies (200,300, and 400mJ) from the two different Ti targets bulk, and nano, respectively. The emitted lines were matched with the atomic titanium standard lines (Ti I) and ionic titanium standard lines (Ti II) [17]. The higher intensity for the atomic lines compared with the ionic

ones indicates a low degree of ionization as a characteristics of cold plasma.

In general, the emission lines intensities increase with increasing the laser energy as a result of increasing the ablated material due to increasing the sputtering yield per pulse with increasing falling energy at small period. These ablated and excited atoms act as sources with more photons after de-excitation process. The

different lines of different intensities due to their variation in probability of transitions and the statistical weight of the upper energy levels. The increasing in intensity with increasing energy is not the same for all lines due to the variation in plasma temperature which cause variation in electronic distributions for energy levels as shown by Boltzmann distribution [18]. From the other hand the lines intensity higher and more clear using the nano target compare with the bulk and micro targets. Also, exposing the spectral lines be more broadening for the nano sample, which indicates on increasing the plasma density according to Stark's principle [19]. The high probability of breakdown on the target surface of nanoparticles because these nanoparticles can act as thermally insulated from the surrounded, so the heating process cause rapidly evaporation of sublimation the nanoparticles [20]

The number of emitters in the plasma increases depending on the amount of material removed by the electromagnetic field of the laser. The generation of the seed electron necessary for plasma induction is greatly influenced by the strengthening of the electromagnetic field during the laser-matter interaction. The Keldysh parameter makes it easy to determine whether the ionization of atoms in a sample occurs by tunneling of the work function barrier via field emission or by absorption of photons, that is,

whether electrons escape through direct or indirect modes of ionization [7].

$$\gamma = \omega \frac{\sqrt{m_e V_B}}{eE} \dots\dots\dots (5)$$

where V_B is the work function potential, E is the electric field intensity, ω is the laser frequency and m_e and e are the electron mass and charge, respectively. If $\gamma > 1$, the ionization occur by multiphoton ionization; while, if $\gamma < 1$, the field emission is the main mechanism.

The Keldysh parameter (γ) was determine for our experiment condition as follows:

- Laser wavelength $\lambda = 1064 \text{ nm} \rightarrow$ light frequency $= 2.82 \times 10^{14} \text{ Hz}$
- Incident energy 200, 300, 400 mJ per 10 ns on 2 mm spot diameter \rightarrow light intensity $I = 6.37 \times 10^{12}$, 9.55×10^{12} and $1.27 \times 10^{13} \text{ W/m}^2$
- The electric field determine according to $I = \frac{1}{2} \epsilon_0 |E_{rms}|^2 c \rightarrow E = 6.93 \times 10^7$, 8.48×10^7 , and $9.79 \times 10^7 \text{ V/m}$, respectively
- The Ti work function $= 4.33 \text{ eV}$ then using equation (5) $\rightarrow \gamma = 20.22$, 16.49 , and 14.27

The high values of Keldysh parameter indicate that the ionization occur by multiphoton process. These formation of seed electrons is the crucial point to enhance the breakdown and so enhance the plasma emission.

Figure 4: spectra from bulk Ti target under 8×10^{-2} Torr vacuum at different laser energies

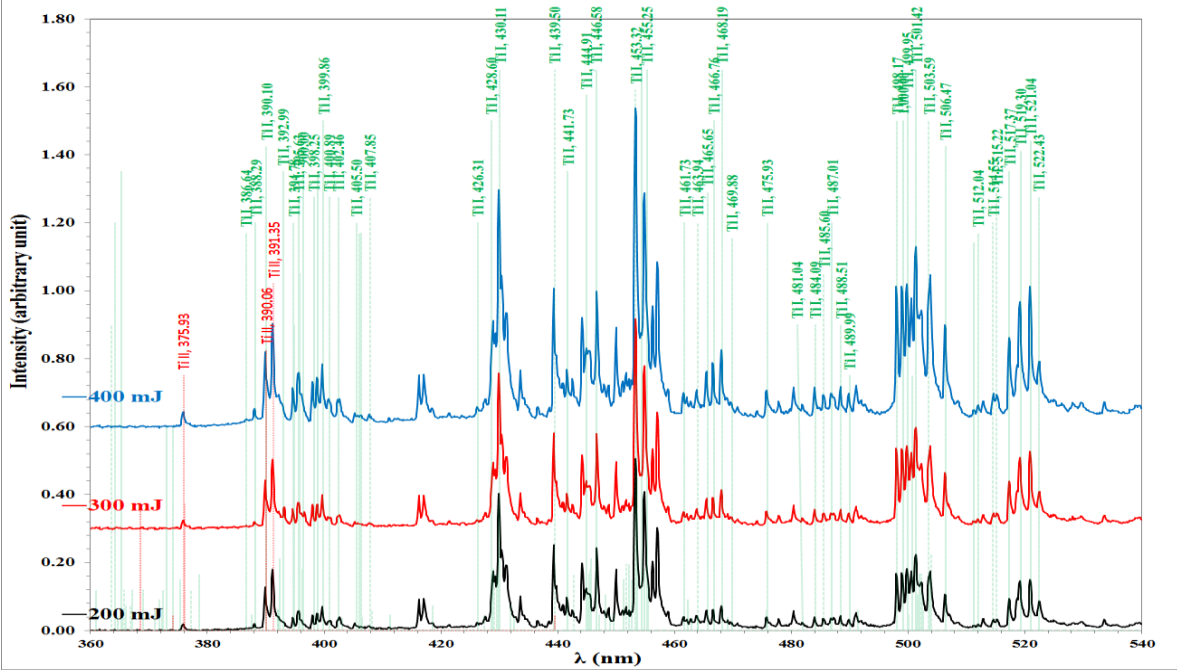
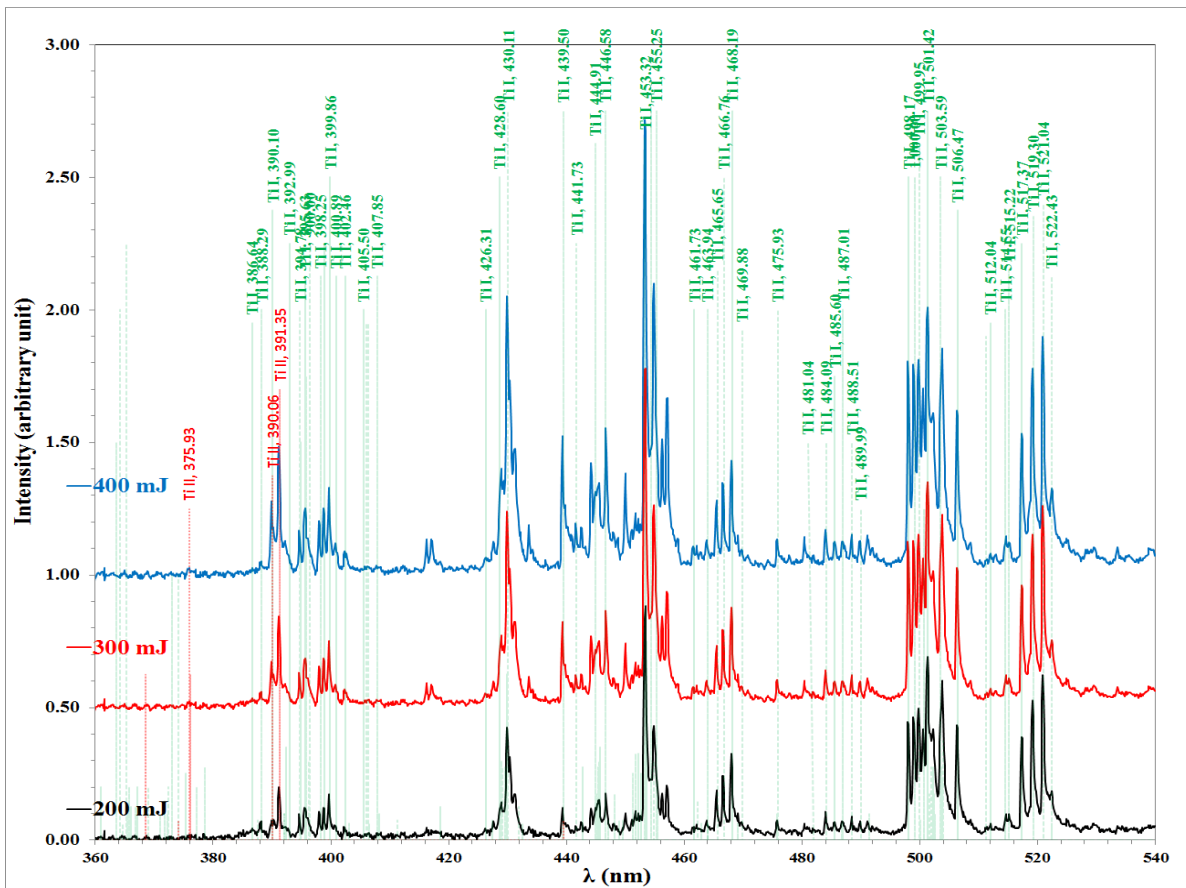
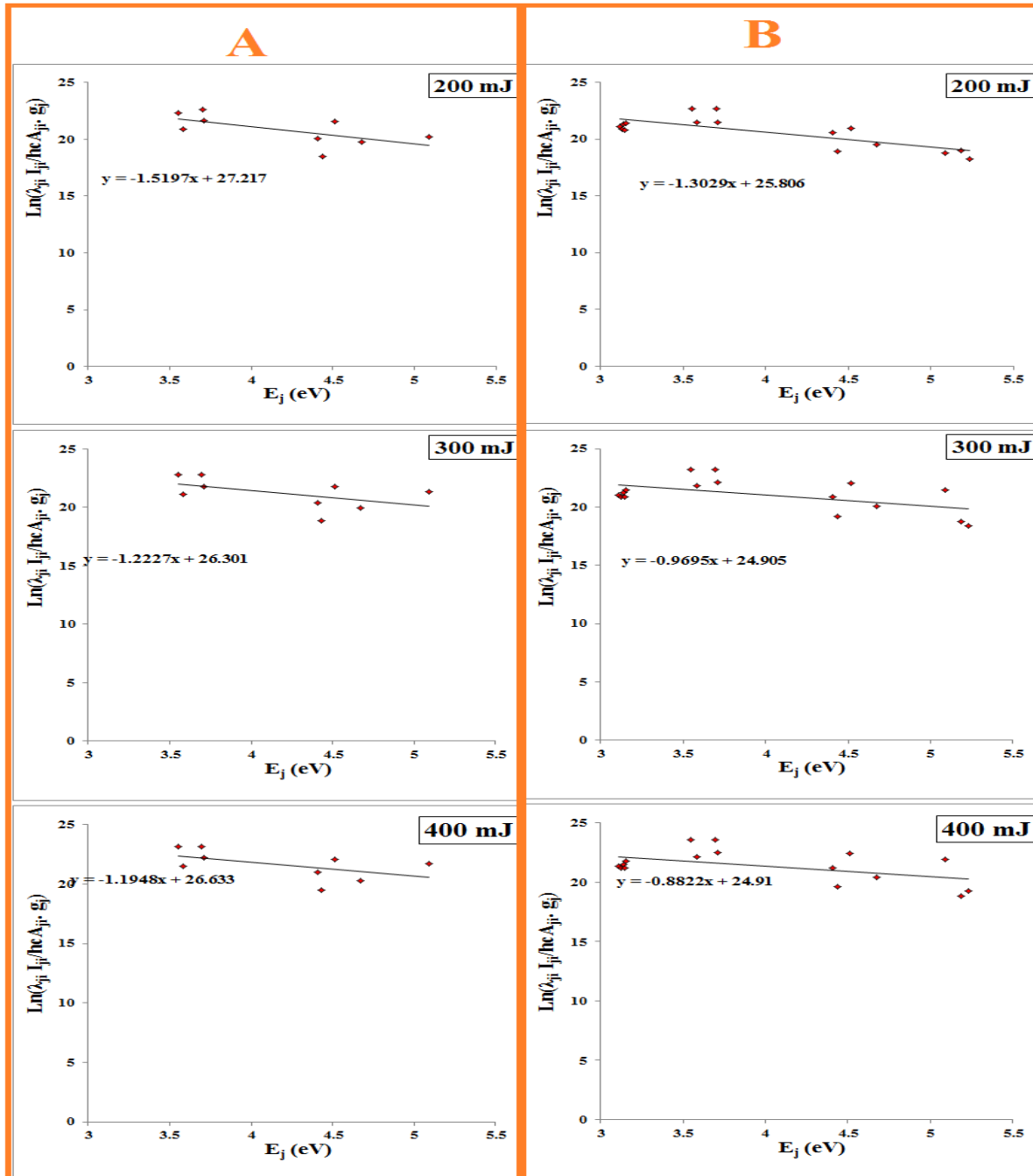


Figure 5: spectra from nano Ti target under 8×10^{-2} Torr vacuum at different laser energies



Electron temperature (T_e) were determined by Boltzmann-Plot (Figure 6), while the electron density (n_e) for the different laser energies onto the different targets were determined according to Saha-Boltzmann relation (equation 2.7).

Figure 6: Boltzmann plot for Ti I emitted lines using different laser energies in 8×10^{-2} Torr air from (A) bulk, and (B) nano- targets.



The variation of electron temperature (T_e) and electron density (n_e) with the laser energy for the three different targets under 8×10^{-2} vacuum from the three different targets were shown in Figure 7. Both T_e and n_e increased with increasing the laser energy. From the other

hand, there are small variation in T_e for the different targets, and increasing the n_e for the nano-targets compare with the other two targets as a result the enhancement of ionization by photon absorption for the nanoparticles.

Figure 7: variation of electron density and plasma temperature with laser energies under 8×10^{-2} Torr from (A) bulk , and (B) nano- targets.

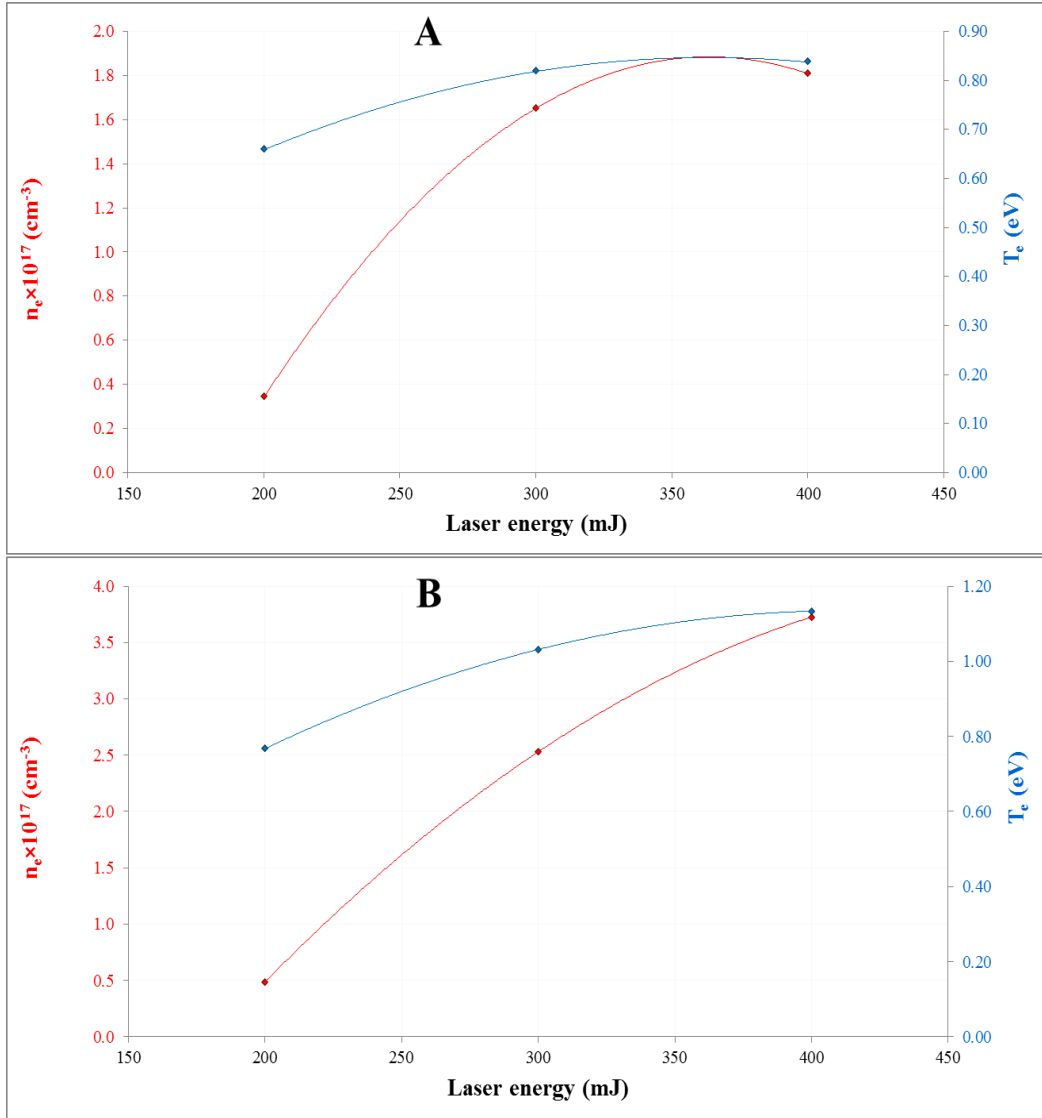


Table 3 listed the plasma parameters induced by different laser energies at 8×10^{-2} Torr vacuum pressures from the different target

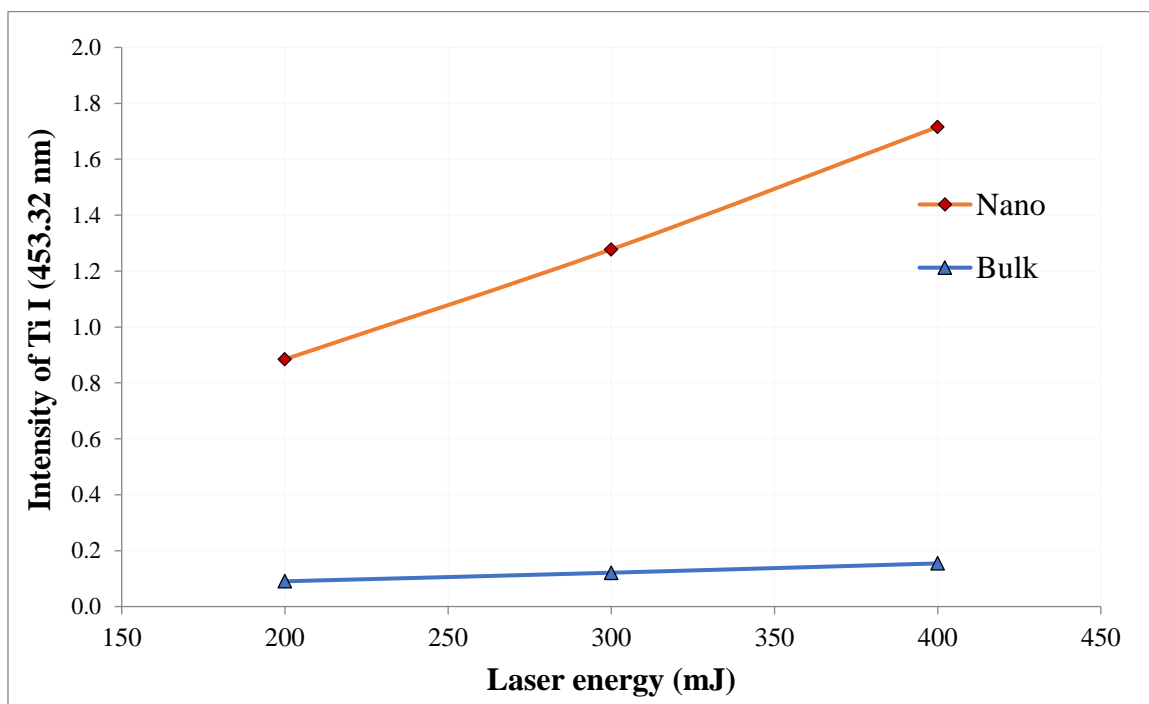
configurations. It seem the plasma parameters satisfied the plasma criteria.

Table 3: plasma parameters induced by different laser energies from bulk, and nano- targets

Sample	E (mJ)	T_e (eV)	$n_e \times 10^{17}$ (cm ⁻³)	$f_p \times 10^{12}$ (Hz)	$\lambda_D \times 10^{-5}$ (cm)	N_d
Bulk	200	0.658	0.34	1.659	3.262	4963
	300	0.818	1.65	3.648	1.654	3128
	400	0.837	1.81	3.818	1.599	3094
Nano	200	0.768	0.49	1.981	2.951	5238
	300	1.031	2.53	4.517	1.500	3578
	400	1.134	3.73	5.482	1.296	3397

The emission intensity for LIPS at different experimental parameters were studied employing the intensity of 453.32 nm wavelength Ti-I line, as illustrated in Figure 8.

The line intensity increased with increasing the laser energy, increased from bulk to micro to nano targets.

Figure 8: variation of emission intensity of Ti I (453.32 nm) with laser energies under 8×10^{-2} Torr vacuum pressures from the two different targets.

4. Conclusions

The target configuration of the titanium metal, as nano or bulk, highly affects the plasma parameters induced by a laser as a result of the variation in the mechanism of laser-matter interaction. Variation of laser energy may cause variation in the generation mechanism of seeds electron so variation in the breakdown is induced. The plasma density enhanced for the plasma-induced from the nano-target compared with the bulk one, while the plasma temperature slightly increased. The nano-target enhanced the emission intensity compared with the bulk target. This technique is a candidate for enhancing the LIPS intensity for small targets and low absorption targets without causing inner cracks by deposition of the nanoparticle on the target surface.

References

- M. W. Morooka, J. E. Wahlund, D. J. Andrews, A. M. Persoon, S. Y. Ye, W. S. Kurth, D. A. Gurnett, and W. M. Farrell, "The Dusty Plasma Disk Around the Janus/Epimetheus Ring," *J. Geophys. Res. Sp. Phys.*, vol. 123, no. 6, pp. 4668–4678, 2018.
- C. Cardinaud, "Fluorine-based plasmas: Main features and application in micro-and nanotechnology and in surface treatment," *Comptes Rendus Chim.*, vol. 21, no. 8, pp. 723–739, 2018.
- H. C. Kim, F. Iza, S. S. Yang, M. Radmilović-Radjenović, and J. K. Lee, "Particle and fluid simulations of low-temperature plasma discharges: benchmarks and kinetic effects," *J. Phys. D. Appl. Phys.*, vol. 38, no. 19, pp. R283–R301, 2005.
- A. A. Menazea, "Femtosecond laser ablation-assisted synthesis of silver nanoparticles in organic and inorganic liquids medium and their antibacterial efficiency," *Radiat. Phys. Chem.*, vol. 168, p. 108616, 2020.
- M. Z. Butt, "Laser ablation characteristics of metallic materials: Role of Debye-Waller thermal parameter," *IOP Conf. Ser. Mater. Sci. Eng.*, vol. 60, no. 1, p. 012068, 2014.
- A. W. Miziolek, V. Palleschi, and I. Schechter, Eds., "History and fundamentals of LIBS," in *Laser-Induced Breakdown Spectroscopy (LIBS)*, Cambridge: Cambridge University Press, pp. 1–39.
- A. De Giacomo, R. Gaudiuso, C. Koral, M. Dell'Aglio, and O. De Pascale, "Nanoparticle Enhanced Laser Induced Breakdown Spectroscopy: Effect of nanoparticles deposited on sample surface on laser ablation and plasma emission," *Spectrochim. Acta Part B At. Spectrosc.*, vol. 98, pp. 19–27, 2014.
- S. Marino, S. Palanco, M. Gabás, R. Romero, and J. R. Ramos-Barrado, "Laser nano- and micro-structuring of silicon using a laser-induced plasma for beam conditioning," *Nanotechnology*, vol. 26, no. 5, p. 055303, 2015.
- A. M. EL Sherbini, A. E. EL Sherbini, C. G. Parigger, and T. M. EL Sherbini, "Nanoparticle enhancement of diagnosis with Laser-Induced plasma spectroscopy," *J. Phys. Conf. Ser.*, vol. 1253, no. 1, p. 012002, 2019.
- M. Fikry, W. Tawfik, and M. M. Omar, "Investigation on the effects of laser parameters on the plasma profile of copper using picosecond laser induced plasma spectroscopy," *Opt. Quantum Electron.*, vol. 52, no. 5, p. 249, 2020.
- S. K. Hameed, N. A. Razzak, A. F. Mahood, and K. L. Nahi, "Optical Emission Spectroscopy of Laser-Produced Plasmas of Some Metal Targets," *Iraqi J. Appl. Phys.*, vol. 18, no. 1, pp. 15–20, 2022.
- "NIST Chemistry WebBook, U.S. department of commerce, on line available."

- W. H. Bragg and W. L. Bragg, *X Rays and Crystal Structure*. London: G. Bell and Sons, LTD., 1918.
- P. Scherrer, "Göttinger Nachrichten Gesell," *Univ. zu Göttingen*, vol. 2, p. 98, 1918.
- M. Shaheera, K. G. Girija, M. Kaur, V. Geetha, A. K. Debnath, R. K. Vatsa, K. P. Muthe, and S. C. Gadkari, "Characterization and device application of indium doped ZnO homojunction prepared by RF magnetron sputtering," *Opt. Mater. (Amst)*, vol. 101, p. 109723, 2020.
- D. Raha and D. Das, "Nanocrystalline silicon thin films prepared by low pressure planar inductively coupled plasma," *J. Appl. Surf. Sci.*, vol. 276, pp. 249–257, 2013.
- "NIST Atomic Spectra Database." [Online]. Available:
<http://kinetics.nist.gov/index.php>.
- F. Bredice, P. Pacheco Martinez, C. Sánchez-Aké, and M. Villagrán-Muniz, "Temporal evolution of the spectral lines emission and temperatures in laser induced plasmas through characteristic parameters," *Spectrochim. Acta Part B At. Spectrosc.*, vol. 107, pp. 25–31, 2015.
- B. Zmerli, B. Nessib, and M. S. Dimitrijevi, "On the Stark broadening of CuI spectral lines," vol. 15, pp. 152–156, 2010.
- S. Hashimoto, D. Werner, and T. Uwada, "Studies on the interaction of pulsed lasers with plasmonic gold nanoparticles toward light manipulation, heat management, and nanofabrication," *J. Photochem. Photobiol. C Photochem. Rev.*, vol. 13, no. 1, pp. 28–54, 2012.